Computing the Phase Shift

Eller noe slikt

Erlend Lima

October 21, 2020

Abstract

Contents

1. Introduction

The interactions between nucleons is [fullfør] In contrast to the electromagnetic force, there is no fundamental theory of the strong force. As the quarks and gluons dance together within nuclei, their strong interaction leaks out as the residual nuclear force, binding the nucleons together. As such, the nucleon-nucleon interaction must be described by approximations and phenomenological models.

The phase shift is a useful proxy for understanding nucleon-nucleon interaction, acting as a bridge between empirically obtained cross sections and theoretical models. Among these theoretical tools to compute the phase section are the K-matrix theory and the variable phase approach (VPA). Both of these are herein investigated by applying them to a two-nucleon system, implemented in the https://julialang.org/.

2. Theory

Quantum scattering is a very complicated process, behaving so differently from the classical case of billiard balls that our intuition breaks down. Fortunately, the intricacies of the scattering process itself can be conveniently omitted by instead focusing on the relationship between the initial and resulting states, illustrated in FIGURE. Specifically, the true state $|\psi\rangle$ is related to the asymptotic incoming and outgoing states $|\psi_{\text{in}}\rangle$ and $|\psi_{\text{out}}\rangle$ through the so-called Møller operators $\Omega_\pm$:

$$|\psi\rangle = \Omega_+ |\psi_{\text{in}}\rangle = |\phi+\rangle$$
$$|\psi\rangle = \Omega_- |\psi_{\text{out}}\rangle = |\phi-\rangle .$$

[Add some history of Møller]

If time dependence is added, the Møller operations allows one to move between the asymptotic states and the actual state at time t. Combining them, the outgoing state is related to the incoming state by

$$|\psi_{\text{out}}\rangle = \Omega_-^\dagger \Omega_+ |\psi_{\text{in}}\rangle = \mathcal{S} |\psi_{\text{in}}\rangle$$

giving the definition of the scattering operator $\mathcal{S}$. In the general case, let $|\chi-\rangle$ and $|\Phi+\rangle$ be any arbitrary orbits. The probability of the process $|\Phi+\rangle \to |\chi-\rangle$ occurring is then the square of the matrix element of $\mathcal{S}$:

$$w(\chi \leftarrow \Phi) = |\langle \chi-|\Phi+\rangle|^2 = |\langle \chi|\mathcal{S}|\Phi\rangle|^2 .$$

While the probability w itself is not observable, the related quantity cross-section $\sigma(\chi \leftarrow \Phi)$ is. The outgoing particle can scatter into a solid angle $d\Omega$, oriented in the direction of momentum $\vec{p}$. Likewise, the incoming particle can be described as wave packets with narrowly defined momentum $\vec{p_0}$. It can then be shown[1, p. 51] that the differential cross section is

$$\frac{\mathrm{d}\sigma}{\mathrm{d}\Omega} = |f(\vec{p} \leftarrow \vec{p_0})|^2$$

with $f(\vec{p} \leftarrow \vec{p_0})$ being the scattering amplitude, as known from elementary scattering theory. Note that only the magnitude of f can be obtained through the cross-section.

The next step is to relate cross-section to the scattering operator. It can be shown[t]hat $\mathcal{S}$ commutes with the free Hamiltonian $\mathcal{H}_0$

$$\mathcal{H} = \mathcal{H}_0 + V \qquad [\mathcal{H}_0, \mathcal{S}] = 0$$

Letting $|p\rangle$ be the eigenvectors of $\mathcal{H}_0$ in momentum basis, we have

$$\langle p'|[\mathcal{H}_0, \mathcal{S}]|p\rangle = (E_{p'} - E_p)\langle p'|\mathcal{S}|p\rangle = 0$$

implying that $\langle p'|\mathcal{S}|p\rangle$ is zero except for $E_{p'} = E_p$. This leads to the form

$$\langle p'|\mathcal{S}|p\rangle = \delta(E_{p'} - E_p) \times \text{remainder}$$

At this point it is fruitful to define a new operator $\mathcal{R} \equiv 1 - \mathcal{S}$. $\mathcal{R}$ is the difference between the case of scattering and no scattering. It too commutes with $\mathcal{H}_0$, and so has the form

$$\langle p'|\mathcal{R}|p\rangle = -2\pi i \delta(E_{p'} - E_p) t(p' \leftarrow p)$$

with the factors $-2\pi i$ and $t(p' \leftarrow p)$ introduced for future convenience. The elements of $\mathcal{S}$ can therefore be written

$$\langle p'|\mathcal{S}|p\rangle = \delta(p' - p) - 2\pi i \delta(E_{p'} - E_p) t(p' \leftarrow p).$$

The function $t(p' \leftarrow p)$ is continuous for most potentials and analytic for many, but only defined for the "shell" $p'^2 = p^2$. However unphysical, it is computationally beneficial to define an operator $\mathcal{T}$ whose matrix elements $\langle p'|T|p\rangle$ are defined for all p and coincide with the values of t on the shell.

The scattering amplitude can be shown to be related to the on-shell $\mathcal{T}$ matrix elements as[1, p. 172]

$$f(p' \leftarrow p) = -(2\pi)^2 m t(p' \leftarrow p).$$

The elements of the scattering matrix can thus be written in terms of the scattering amplitude:

$$\langle p'|\mathcal{S}|p\rangle = \delta(p' - p) - \frac{i}{2\pi m}\delta(E_{p'} - E_p)f(p' \leftarrow p).$$

The first term describes the situation where no scattering occurs, while the second is the amplitude for when the wave is actually scattered, with the probability being the square of the scattering amplitude, hence its name.

2.1. Spherical Coordinates

Introducti

As known from elementary quantum mechanics, $\mathcal{H}^0$ commutes with the angular momentum operator $\mathcal{L}^2$ and z-axis projection $\mathcal{L}_3$. These three operators form a complete set of commuting observables. As $\mathcal{S}$ commutes with $\mathcal{H}^0$, $\mathcal{S}$ too commutes with the aforementioned operators, and is diagonal in the common basis, namely the basis of spherical waves $\{|Elm\rangle\}$, with $E, l(l+1)$ and m being the eigenvalues for $\mathcal{H}^0$, $\mathcal{L}^2$ and $\mathcal{L}_3$ respectively. Since this basis diagonalizes $\mathcal{S}$, its matrix elements in this basis are

$$\langle E'l'm'|\mathcal{S}|Elm\rangle = \delta(E' - E)\delta_{l'l}\delta_{m'm}s_l(E).$$

$\mathcal{S}$ can be shown to be unitary, implying the eigenvalues $s_l(E)$ must have modulus one, justifying the form

$$\langle E'l'm'|\mathcal{S}|Elm\rangle = \delta(E' - E)\delta_{l'l}\delta_{m'm}\exp(2i\delta_l(E))$$

The quantity $\delta_l(E)$ is the important phase shift, an observable obtainable from both experiment and numerical calculations. It is purely real with an inherent ambiguity modulo π, as seen from

$$\exp(2i[\delta_l + n\pi]) = \exp(2i\delta_l)\exp(2in\pi) = \exp(2i\delta_l).$$

[Meaning of T in the sense incident plane wave] []

The decomposition of $f(\mathrm{p}' \leftarrow \mathrm{p})$ into partial waves can be obtained by exploiting the relation

$$\langle \mathrm{p}'|(\mathcal{S}-1)|\mathrm{p}\rangle = \frac{i}{2\pi m}\delta(E' - E)f(\mathrm{p}' \leftarrow \mathrm{p}). \tag{2.1}$$

Inserting a complete set of states of the left hand side gives

$$\langle \mathrm{p}'|(\mathcal{S}-1)|\mathrm{p}\rangle = \int \mathrm{d}E \sum_{l,m} \langle \mathrm{p}'|(\mathcal{S}-1)|Elm\rangle \langle Elm|\mathrm{p}\rangle$$

$$= \int \mathrm{d}E \sum_{l,m} (s_l(E)-1) \langle \mathrm{p}'|Elm\rangle \langle Elm|\mathrm{p}\rangle$$

$$= \frac{1}{mp}\delta(E_{p'} - E_p) \sum_{l,m} Y_l^m(\hat{\mathrm{p}}')[s_l(E_p)-1]Y_l^m(\hat{\mathrm{p}})^*$$

where Y_l^m are the spherical harmonicals and the hat denotes unit vector. Combining this with (2.1), the amplitude can be decomposed to

$$f(\mathrm{p}' \leftarrow \mathrm{p}) = \frac{2\pi}{ip} \sum_{l,m} Y_l^m(\hat{\mathrm{p}}')[s_l(E_p)-1]Y_l^m(\hat{\mathrm{p}})^*$$

Letting $\hat{\mathrm{p}}$ lie along z and noting independence of m [WHY], we define

$$f(E_p, \theta) \equiv f(\mathrm{p}' \leftarrow \mathrm{p}) = \frac{1}{2ip} \sum_l (2l+1)[s_l(E_p)-1]P_l(\cos\theta)$$

This leads to the natural definition of the partial wave amplitude as

$$f_l(E) \equiv \frac{s_l(E)-1}{2ip} = \frac{\exp[2i\delta_l(\theta)]-1}{2ip} = \frac{\exp[2i\delta_l(E)]\sin\delta_l(E)}{p}$$

Analogously the total cross-section can be decomposed into partial wave cross-sections, giving

$$\sigma(p) = \sum_l \sigma_l(p) = \sum_l 4\pi(2l+1)\left|f_l(p)\right|^2 = \sum_l 4\pi(2l+1)\frac{\sin^2\delta_l}{p^2}$$

The magnitude of each partial wave cross-section is from this constrained by the so called unitary bound:

$$|\sigma_l| \le 4\pi\frac{2l+1}{p^2}.$$

The maximal value is only reached if δ_l is an odd multiple of $\pi/2$

General properties of the scattering process can be found by studying both the general and the limiting forms of the wave function. As before, the wave function of the full Hamiltonian $\langle vbx|Elm+\rangle$ can be obtained from the wave function of the free Hamiltonian by the Møller operator

$$\langle x|Elm+\rangle = \Omega_+ \langle x|Elm\rangle,$$

and hence we can get away with studying the free wave. From basic quantum mechanics, we know it is on the form $\frac{1}{r}y(r)Y_l^m(\hat{x})$ with $y(r)$ satisfying the radial Schrödinger equation

$$\left[\frac{d^2}{dr^2} - \frac{l(l+1)}{r^2} + p^2\right]y(r) = 0.$$

When $r \to 0$, $y(r)$ must go as r^{-l} or r^{l+1}. The latter condition is satisfied by the Riccati-Bessel functions $\hat{j}_l(z) = zj_l(z)$. Its limiting behavior as $z \to 0$ is

$$\hat{j}_l(z) \xrightarrow[z\to0]{} \frac{z^{l+1}}{(2l+1)!!}\left[1+\mathcal{O}(z^2)\right]$$

The other limiting condition is satisfied by the Riccati-Neumann function $\hat{n}_l(z)$.

Hence

$$\langle x|Elm\rangle = i^l\left(\frac{2m}{\pi p}\right)^{1/2}\frac{1}{r}\hat{j}^l(pr)Y_l^m(\hat{x}) \tag{2.2}$$

On the other side, the limit $r \to \infty$ requires the boundary conditions $e^{\pm ipr}$. These are satisfied by the Riccati-Hankel functions $\hat{h}_l^\pm(z) = \hat{n}_l(z) \pm ij_l(z)$. Its limiting form is

$$\hat{h}_l^\pm(z) = e^{\pm i(z-l\pi/2)}\left[1+\mathcal{O}(z^{-1})\right]$$

In analogy to (2.2), the full wave function can be written as

$$\langle x|Elm+\rangle = i^l\left(\frac{2m}{\pi p}\right)^{1/2}\frac{1}{r}\psi_{lp}(r)Y_l^m(\hat{x})$$

from which we see that $\psi_{lp}(r) \to \hat{j}_l(pr)$ when $V \to 0$. In the other limiting case $r \to \infty$, it can be shown [1, p. 187] to be

$$\psi_{lp}(r) \xrightarrow[r\to\infty]{} \hat{j}_l(pr) + pf_l\hat{h}_l^+(pr).$$

Using the limiting forms of the functions and some algebra, this can be rewritten as

$$\psi_{lp}(r) \xrightarrow[r\to\infty]{} e^{i\delta_l(p)}\sin\left[pr - \frac{1}{2}l\pi + \delta_l(p)\right]$$

This makes significance of the phase shift apparent. At large r the actual wave function becomes proportional to the free wave function

$$\hat{j}_l(pr) \to \sin\left(pr - \frac{1}{2}l\pi\right)$$

except that its oscillations are shifted by the phase shift δ_l.

2.2. Green's Function

One of the most important tools in scattering theory is the resolvent, or Green's operator. For many types of integral equations, a Green's function can be associated, transforming the solving of the equation to the computation of the Green's function. For our purposes the most important Green's operators are the free Green's operator

$$\mathcal{G}^0(z) \equiv (z - \mathcal{H}^0)^{-1}$$

and the full Green's operator

$$\mathcal{G}(z) \equiv (z - \mathcal{H})^{-1}$$

with $z \in \mathbb{C}$. Without loss of generality, assume the spectrum of $\mathcal{H}$ is discrete, with the orthonormal basis $|n\rangle$. Then the full Green's operator can be written

$$\mathcal{G}(z) = (z - \mathcal{H})^{-1}\mathbb{1} = \sum_n \frac{|n\rangle\langle n|}{z - E_n}.$$

A specific matrix element is therefore

$$\langle\chi|\mathcal{G}(z)|\psi\rangle = \sum_n \frac{\langle\chi|n\rangle\langle n|\psi\rangle}{z - E_n}.$$

For any z not an eigenvalue E_n, the matrix element is well defined and analytic. When z is an eigenvalue, it is a simple pole with residue $\langle\chi|n\rangle\langle n|\psi\rangle$. That is, knowing the poles of $\mathcal{G}(z)$ gives information about the corresponding eigenvectors. As both the energy eigenvectors and eigenvalues can be found from $\mathcal{G}(z)$ itself, knowledge of $\mathcal{G}(z)$ is equivalent to solving the eigenvalue problem of $\mathcal{H}$[*]

While discrete spectra lead to poles in $\langle\chi|\mathcal{G}(z)|\psi\rangle$, continuous spectra lead to branch cuts. Consider the free Green's operator, which in terms of the angular momentum eigenvectors in analogy to the discrete spectrum has the matrix elements

---

[*]Of course, this is merely an intuitive explanation, not a proof. It can be shown that this is indeed true in the general case, see [1, p. 131]

$$\langle\chi|\mathcal{G}^0(z)|\psi\rangle = \int_0^\infty \frac{\mathrm{d}E}{z-E}\left\{\sum_{l,m}\langle\chi|Elm\rangle\langle Elm|\psi\rangle\right\}$$

that again gives well-defined functions for $z \notin \mathbb{R}^+$. For any $E^0 > 0$, the integral diverges. This can be seen by taking the difference between approaching the axis from the top and approaching it from the bottom, yielding[2, p. 469] $2\pi i \sum_{lm}|Elm\rangle\langle Elm|$.

The scattering process can yield both scattered states and bound states. The former is associated with continuous spectra while the latter with discrete. From the discussion above, scattered states correspond with branch cuts along $E^0 > 0$ while bound states show up as simple poles in $\mathcal{G}(z)$.

Finding $\mathcal{G}(z)$ is just as difficult as solving the eigenvalue problem for $\mathcal{H}$. Using $\mathcal{G}(z)$, however, yields an alternative numerical approach while at the same providing a powerful theoretical tool. The first step is to write $\mathcal{G}(z)$ in terms of the simpler $\mathcal{G}^0(z)$. This is trivially done using the algebraic relation

$$\mathcal{A}^{-1} = \mathcal{B}^{-1} + \mathcal{B}^{-1}(\mathcal{B}-\mathcal{A})\mathcal{A}^{-1}.$$

Inserting $\mathcal{A} = z - \mathcal{H}$ and $\mathcal{B} = z - \mathcal{H}^0$ gives

$$\mathcal{G}(z) = \mathcal{G}(z)^0 + \mathcal{G}(z)^0 V\mathcal{G}(z) = \mathcal{G}(z)^0 + \mathcal{G}(z)V\mathcal{G}(z)^0. \tag{2.3}$$

This is known as the Lippmann-Schwinger equation for $\mathcal{G}(z)$.

2.3. Lippman Schwinger

The Lippmann-Schwinger equation turns out to be a common and useful relation between operators in scattering theory. The derivation through Green's operators is not the historic path, and has the downside of obscuring its physical relationship to the Schrödinger equation.

[intro] Out of thin air we define the operator $\mathcal{T}$ as the potential plus the distortion to the potential caused by the full Green's operator:

$$\mathcal{T}(z) = V + V\mathcal{G}V. \tag{2.4}$$

It is clear that $\mathcal{T}(z)$ has the same properties as $\mathcal{G}(z)$ with respect to poles and branch cuts. Combining (2.4) with (2.3) together with some algebraic manipulations, we obtain the Lippmann-Schwinger equation for $\mathcal{T}(z)$:

$$\mathcal{T}(z) = V + V\mathcal{G}^0(z)\mathcal{T}(z). \tag{2.5}$$

In momentum space (2.5) is written as

$$\langle \mathrm{p}'|\mathcal{T}(z)|\mathrm{p}\rangle = \langle \mathrm{p}'|V|\mathrm{p}\rangle + \int \mathrm{d}^3 p'' \frac{\langle \mathrm{p}|V|\mathrm{p}''\rangle}{z - E_{p''}}\langle \mathrm{p}''|T(z)|\mathrm{p}\rangle$$

This highlights the need for introducing the $\mathcal{T}$ operator in the first place. There is no LS equation for the $\mathcal{S}$ because it requires the operators to be smooth functions, while $\mathcal{S}(z)$ is highly singular. On the other hand $\mathcal{T}$ analytic almost everywhere, allowing it to be expressed in terms of an integral equation.

Through a long and rather limit-finicky derivation, the $\mathcal{S}$ operator can be derived in terms of the $\mathcal{T}$ operator when z approaches the real axis from above

$$\langle \mathrm{p}'|S|\mathrm{p}\rangle = \delta(\mathrm{p}' - \mathrm{p}) - 2\pi i\delta(E_{p'} - E_p)\lim_{\epsilon\downarrow 0}\langle \mathrm{p}'|T(E_p + i\epsilon)|\mathrm{p}\rangle.$$

This relation being the main motivation for defining $\mathcal{T}$ in the first place. It shows that $t(\mathrm{p}' \leftarrow \mathrm{p})$ corresponds to the on-shell T-matrix.

A reasonable question to ask is why computing the entire T-matrix is necessary when only the on-shell elements are physical. As already mentioned, one reason is computational; The on-shell elements are the limiting quantities of the off-shell elements. This doesn't mean that the off-shell elements are only a mathematical necessity. In fact, they correspond to the virtual interactions in the scattering process, which accounts for their fundamental unmeasurable nature. We are only allowed to observe the scattering in the non-interacting region, being the limiting case of the unobservable processes happening inside of the interacting region. Our initial starting point of focusing on the asymptotic states while ignoring the intricacies of the scattering is therefore not some mathematical trick to make computation easier, but an unavoidable requirement.

2.4. The K-Matrix

The Lippmann-Schwinger equation for $\mathcal{T}$ can not be solved by simple analytical methods. One recourse is to use approximation techniques. These are based on the expansion of $\mathcal{T}$ into the infinite sum

$$\mathcal{T} = V + V\frac{1}{E - H^0 + i\epsilon}V + V\frac{1}{E - H^0 + i\epsilon}V\frac{1}{E - H^0 + i\epsilon}V + ...$$

The unitarity condition of $\mathcal{T}$ is satisfied for the whole series, but violated for any finite order. If the series happens to be rapidly convergent, it may not pose a problem for numerical methods[†]. Nevertheless, a more stable approach is to enforce unitarity. The Caley transform achieves this, whereby a Hermitian operator is constructed in such a way as to ensure unitary.

The Caley transform of $\mathcal{S}$ is denoted by $\mathcal{K}$, and is defined as

$$\mathcal{K} = i\frac{1 - \mathcal{S}}{1 + \mathcal{S}}.$$

The K-matrix[‡] is the matrix elements of the $\mathcal{M}$ operator:

$$\langle \mathrm{p}'|\mathcal{K}|\mathrm{p}\rangle = \delta(E_{p'} - E_p)k(\mathrm{p}' \leftarrow \mathrm{p}).$$

[†]That is to say, if the process described is sufficiently elastic, energy will be approximately conserved and convergence will be rapid. [3]

[‡]The nomenclature of the K-matrix is a mess. It is also called the R-matrix, the T-matrix, the reaction matrix, the reactance matrix, the damping matrix, the distortion matrix, the dissipative matrix, and Heitler's matrix. To avoid overworking any of the other letters, I follow the style of Taylor.

The advantage of $\mathcal{K}$ is that as long as it is Hermitian, $\mathcal{S}$, and by consequence $\mathcal{T}$, is guaranteed to be unitary. This property also holds for any Hermitian $\tilde{\mathcal{K}}$ that is not the true $\mathcal{K}$ of a scattering problem, for example due to numerical errors[4, 5].

From our definition of $\mathcal{R} = \mathcal{S} - 1$, the follows readily that

$$\mathcal{R} = 2i\mathcal{K} + iM\mathcal{R}.$$

By taking the matrix elements we obtain the Heitler's damping equation

$$-\pi t(\mathrm{p}' \leftarrow \mathrm{p}) = k(\mathrm{p}' \leftarrow \mathrm{p}) - \pi i \int \mathrm{d}^3 p\, k(\mathrm{p}' \leftarrow \mathrm{p}'')\delta(E_{p''} - E_p)t(\mathrm{p}'' \leftarrow \mathrm{p}).$$

The functions $t(\mathrm{p}' \leftarrow \mathrm{p})$ are as known the on-shell matrix elements of the $\mathcal{T}$ operator, and $\mathcal{T}$ has a related Lippmann-Schwinger equation (2.5). Heitler's damping equation allows us to substitute $\mathcal{K}$ for $\mathcal{T}$, giving the Lippmann-Schwinger equation for K[§]:

$$K = V + VP\mathcal{G}^0 K \qquad\qquad *$$

where P denotes the principal value. The equivalent matrix element form for a central and spherically symmetric potential is[morten]

$$\langle p'|K|p\rangle = \langle p'|V|p\rangle + \frac{2}{\pi}\int_0^\infty dp''\,\langle p'|V|p''\rangle \frac{1}{E - p''/m}\langle p''|K|p\rangle. \qquad (2.6)*$$

This equation provides a numerically stable method to find the matrix K.

When $\mathcal{S}$ is symmetric, $\mathcal{K}$ is both Hermitian and symmetric, implying its matrix elements are real. As with $\mathcal{S}$ and $\mathcal{R}$, $\mathcal{K}$ becomes diagonal in the basis $\{|Elm\rangle\}$:

$$\langle E'l'm'|\mathcal{S}|Elm\rangle = \delta(E_{p'} - E_p)\delta_{l',l}\delta_{m',m}s_l(E)$$
$$\langle E'l'm'|\mathcal{R}|Elm\rangle = \delta(E_{p'} - E_p)\delta_{l',l}\delta_{m',m}2ipf_l(E)$$
$$\langle E'l'm'|\mathcal{M}|Elm\rangle = \delta(E_{p'} - E_p)\delta_{l',l}\delta_{m',m}k_l(E).$$

The elements $k_l(E)$ will in this case be real, and are directly related to the phase shifts:

$$k_l = i\frac{1 - s_l}{1 + s_l} = -\frac{1}{p}\tan\delta_l. \qquad\qquad *$$

That is, finding K by solving (2.6) lets us directly obtain the phase shift from the diagonal elements of K, and will be one of our two methods to compute the phase shift.

As a side note, the K-matrix is related standing wave stationary states in the same fashion that the T-matrix is related to plane wave stationary states. This is seen by writing the principal value of the Green's operator as

$$P\mathcal{G}^0 = P\frac{1}{E - \mathcal{H}^0} = \lim_{\varepsilon \to 0}\frac{1}{2}\left[\frac{1}{E - \mathcal{H}^0 + i\varepsilon} + \frac{1}{E - \mathcal{H}^0 - i\varepsilon}\right].$$

This is the Green's operator of an incoming wave and an outgoing wave, resulting in standing waves.

[§]The astute reader will notice that there are some factors $-i$, π and p missing. Their definitional absence makes results involving the reactance matrix more readable, but requires redefining $\mathcal{R}$ and $\mathcal{T}$, which in turn would make other results ugly. As the factors are ultimately irrelevant, I decided to ignore them and instead annotate the concerning equations with $*$. Compare e.g. [morten, 1, 5] or any other reference for the total train wreck that otherwise ensues.

2.5. The Variable Phase Approach

An alternative way to compute the phase shift is through the variable phase approach (VPA). To develop it, it is useful to introduce another partial wave function $\phi_{lp}(r)$ that differs from $\psi_{lp}(r)$ only in its normalization. It is defined as the solution to the radial Schrödinger equation that behaves exactly as $\hat{j}_l$ as $r \to 0$,

$$\psi_{lp}(r) \xrightarrow[r \to 0]{} \hat{j}_l(pr)$$

Since both the boundary condition and the radial equation are real, $\psi_{lp}(r)$ is always real, hence its name the regular solution.

The VPA method is based on approximating the regular solution of a potential by the regular solution to a truncated potential. As such, different equations are necessary for different l, so we will only look at s-waves. Define the truncated potential $V_\rho(r)$ by

$$V_\rho = \begin{cases} V(r) & r \le \rho \\ 0 & r > \rho \end{cases}$$

The regular solution to the full potential is $\psi(r)$, while for the truncated potential it is $\psi_\rho(r)$. Likewise, the true phase shift is δ, and the phase shift for the truncated potential is $\hat{\delta}(\rho)$. The inherent modulo π ambiguity in $\delta(\rho)$ is removed by defining $\delta(0) = 0$. As ρ increases, it is clear that the truncated potential approximates the true potential, hence

$$\delta(\rho) \xrightarrow[\rho \to \infty]{} \delta$$

For $r \le \rho$, both regular solutions coincide[¶]:

$$\psi(r) = \psi_\rho(r) \qquad r \le \rho.$$

The truncated regular solution is given by

$$\phi_\rho(r) = \alpha(\rho) \sin\left[pr + \delta(\rho)\right],$$

for $\alpha(\rho)$ some coefficient. As $\phi_\rho(r)$ and $\phi(r)$ coincide for $r = \rho$, we have

$$\phi(\rho) = \alpha(\rho) \sin\left[p\rho + \delta(\rho)\right].$$

This too holds for the derivative at that point, so

$$\phi'(\rho) = p\alpha(\rho) \cos\left[p\rho + \delta(\rho)\right].$$

The choice of ρ is arbitrary, therefore the two relations hold for any ρ and the variable can be substituted with r. Inserting them into the radial Schrödinger equation results in the VPA differential equation for s-waves:

$$\delta'(r) = -\frac{2m}{p} V(r) \sin^2\left[pr + \delta(r)\right]. \tag{2.7}$$

[¶]Note the need for the regular solutions. The normalized solutions $\psi_{lp}(r)$ have different normalizations for different ρ, resulting in different values at r for different truncations.

Not only does the differential equation give a mean to calculate the phase shift, it also gives some theoretical insights. The derivative of the phase shift is the potential V times some negative quantity $-\frac{2m}{p}\sin^2(\cdots)$. If the potential is purely negative, the derivative will be purely positive, and opposite for a purely positive potential. By definition $\delta(r=0)=0$, hence a negative potential yields a positive phase shift, and a positive potential yields a negative phase shift.

2.6. Levinson's Theorem

The regular solutions $\psi_{l,p}(r)$ have already proved themselves as a useful tool in obtaining the phase shift numerically. It is however a gift that keeps on giving, and will now be used to derive[‖] Levinson's theorem, stating that the phase shift in the limit $p \to 0$ equals the number of bound states n_l times π.

As $r \to \infty$, the regular solution must become proportional to the free solution, namely a combination of $\hat{h}_l^{\pm}$ with some suitable coefficients $\mathcal{J}_l(p)$:

$$\phi_{lp} \xrightarrow[r\to\infty]{} \frac{i}{2}\left[\mathcal{J}_l(p)\hat{h}_l^-(pr) - \mathcal{J}_l(p)^*\hat{h}_l^+(pr)\right]. \tag{2.8}$$

One of the asymptotic forms of the normalized solution is

$$\psi_{lp}(r) \xrightarrow[r\to\infty]{} \frac{i}{2}\left[\hat{h}_l^-(pr) - s_l(p)\hat{h}_l^+(pr)\right].$$

Comparing the two equations, we see that

$$s_l = \frac{\mathcal{J}_l(p)^*}{\mathcal{J}_l(p)},$$

and

$$\mathcal{J}_l(p) = \frac{\phi_{lp}(r)}{\psi_{lp}(r)}.$$

The coefficient function $\mathcal{J}_l(p)$ is hence the ratio of the two solutions. It proves to be a very important function, and is called the Jost function. It has an intimate relationship with the scattering matrix, having the same phase with opposite sign as s_l

$$\mathcal{J}_l(p) = |\mathcal{J}_l(p)|\exp\{-i\delta_l(p)\}.$$

The Jost function is a function of the momentum, and to study its behavior, it is necessary to expand the momentum to become a complex variable. Although only real momenta are physical, using the beauty of the complex plane we can retrieve physical insights.

The matrix elements s_l are meromorphic, i.e. analytic everywhere except at a finite number of points[**]. The poles in the upper and lower parts of the complex plane turn out to behave very differently, describing respectively bound states and resonances.

Restricting ourselves to the upper half plane, we can show that the poles of s_l correspond to bound states. For most potentials the relation $\mathcal{J}_l(p)^* = \mathcal{J}_l(-p)$ holds. If the Jost function

---

[‖]I say "derive". What follows is more of a proof sketch than a rigorous treatment, but will hopefully provide the intuition for the truth of the theorem.

[**]This is strictly only true for nice potentials. For our purposes we can pretend that all potentials are so nice. See [1, p. 220] for a more in-depth description.

vanishes for all $p \geq \bar{p}$, then we see from (2.8) that the regular solution will be an exponentially decreasing function above $\bar{p}$

$$\phi_{l\bar{p}} \xrightarrow[r\to\infty]{} -\frac{i}{2}\mathcal{J}_l(p)^* \hat{h}_l^+(pr).$$

As $\phi_{l\bar{p}}(r)$ vanishes at $r = 0$ by definition, it follows that it is in fact normalizable and hence a solution to the radial Schrödinger equation with energy $\frac{\bar{p}}{2m}$. The eigenvalues of the Hamiltonian are real, meaning $\bar{p}$ must be imaginary, $\bar{p} = i\alpha$. The point $\bar{p}$ is therefore a bound state with energy $\frac{-\alpha}{2m}$. The converse is also true[1, p. 224]. As $s_l(p) = \frac{\mathcal{J}_l(p)^*}{\mathcal{J}_l(p)}$, it follows that the when $\mathcal{J}_l(\bar{p}) = 0$, $s_l(\bar{p})$ be a pole corresponding to a bound state. The pole is simple with residue 1.

Levinson's theorem now follows by a simple integration. Consider the contour integral

$$I = \oint_\Gamma \mathrm{d}p \frac{\dot{\mathcal{J}}_l(p)}{\mathcal{J}_l(p)} = \oint_\Gamma \mathrm{d}p \ln \mathcal{J}_l(p)$$

where the contour Γ is a semitorus in the upper half plane. The integrand is analytic except at the n_l zeros of the Jost function, whence it has residue 1. By Cauchy's theorem,

$$I = 2\pi i n_l$$

When the radius of the larger semicircle is larger than $\bar{p}$, its contribution is zero. Taking the limit as the radius goes to infinity, only the path along the real axis plus the smaller semicircle near 0 contributes. On the positive real axis $\mathcal{J}_l(p) = |\mathcal{J}_l(p)| \exp{-i\delta_l(p)}$, so

$$\ln \mathcal{J}_l(p) = \ln|\mathcal{J}_l| - i\delta_l(p),$$

while on the negative real axis it is

$$\ln \mathcal{J}_l(-p) = \ln|\mathcal{J}_l| + i\delta_l(p).$$

Hence the integral evaluates to[††]

$$I = \oint_{-\infty}^{\infty} \mathrm{d}p \ln \mathcal{J}_l(p) + \oint_{\Gamma_\varepsilon} \mathrm{d}p \ln \mathcal{J}_l(p)$$

$$= 2i[\delta_l(0) - \delta(\infty)] + \oint_{\Gamma_\varepsilon} \mathrm{d}p \ln \mathcal{J}_l(p)$$

The small semicircle is slightly tricky due to the Jost functions behavior near 0. With some rigorous treatment is can be coaxed into[1, p. 234]

$$\oint_{\Gamma_\varepsilon} \mathrm{d}p \ln \mathcal{J}_l(p) = \begin{cases} -\pi i & l = 0 \\ -2\pi i & l > 0 \end{cases}$$

Defining $\delta_l(\infty) = 0$ as before, in the end we have for $l = 0$

$$\delta_l(0) = (n_0 + 1/2)\pi,$$

and for $l > 0$

$$\delta_l(0) = n_l\pi,$$

proving Levinson's theorem.

[††]Strictly the contour path consists of the three pieces: $(-\infty, \epsilon)$, Γ_ε and (ε, ∞) along with appropriate limits. Consider this abuse of notation.

2.7. Potentials

2.7.1. The Square Well

Near and dear to everyone is the square well potential; a simple discontinuous potential with value V_0 in the interacting region and zero everywhere else:

$$V(r) = \begin{cases} V_0 & \text{for } 0 \leq r \leq R \\ 0 & \text{for } r > R \end{cases}$$
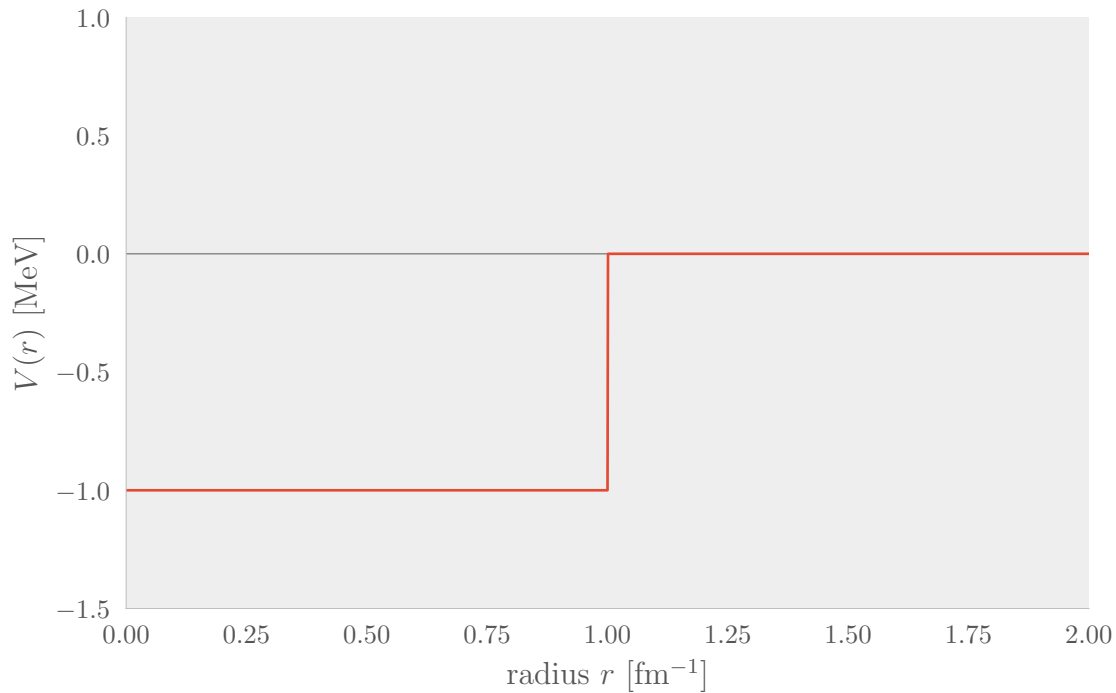
The potential is plotted in Fig. 2.1

Figure 2.1: An attractive square well potential with $V_0 = -1$ MeV.

[Analytical Solutions]

2.7.2. The Yukawa Potential

[HISTORY]

The Yukawa potential was later generalized into a class of generalized Yukawa potentials. They are potentials build on superpositions of Yukawa potentials:

$$V(r) = \sum_{i=1}^{N} C_i \frac{e^{-\eta_i r}}{r}$$

for some coefficients C_i and η_i.

A specific instance of a generalized Yukawa potential is the Reid potential[6]. It was an incremental improvement on already existing potentials at that time, building a parameterized potential where the exponent in each term reflects some phenomenological properties

of the nuclear force while the constants are fit to phase shift data without consideration for their physical interpretation. In the case of proton-neutron scattering, the potential for the partial wave $^1S_0$ consists of the three terms:

$$V(r) = V_a \frac{e^{-ax}}{x} + V_b \frac{e^{-bx}}{x} + V_c \frac{e^{-cx}}{x}$$

where $x = \mu r$, $\mu = 0.7$ MeV, $V_a = -10.463$ MeV, $V_b = -1650.6$ MeV, $V_c = 6484.3$ MeV, and $a = 1$, $b = 4$ and $c = 7$.

The individual terms are plotted in Fig. 2.2 along with their sum. Its construction becomes apparent, where the three terms interact to form its three main features: it is a short range potential, quickly falling off to zero with a range , with an attractive region followed by a strongly repulsive region.
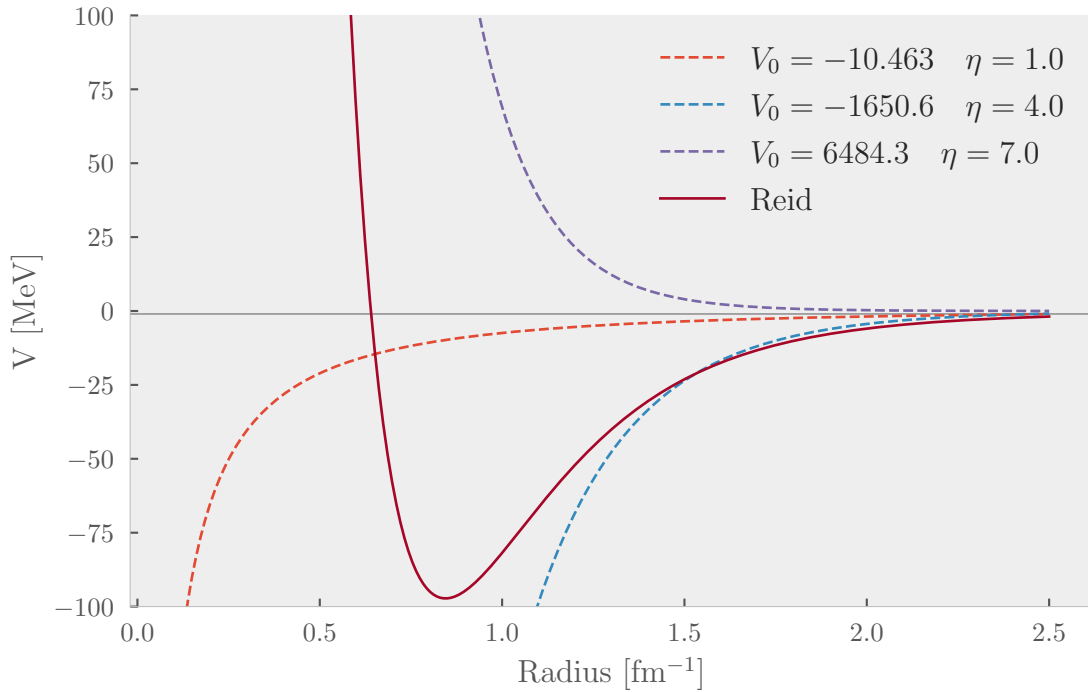
Figure 2.2: The Reid potential (full stroke), a sum of three Yukawa potentials (dashed). It is has the typical characteristics of a nuclear force model, with a short range attractive potential followed by a repulsive core.

The Reid potential for np $^1S_0$ was fit to two thousand data points for the phase shift in the region $0 - 350$ MeV, and thus should provide a good fit in this region.

2.7.3. Momentum Basis

Going from position basis to momentum space requires a change of basis, achieved through a Fourier transform. The problem is multidimensional, requiring a generalized Fourier transform. As we are only dealing with spherically symmetric and central potentials, the more suitable Hankel transform‡‡ can be used. For s-waves, it takes the form:

---

‡‡The Hankel transform can be regarded as the Fourier transform in hyperspherical coordinates, expanding the function in Bessel functions instead of sines and cosines.

$$V(k, k') = \int_0^\infty j_0(kr)V(r)j_0(k'r)r^2 \mathrm{d}r$$

$$= \int_0^\infty \sin(kr)V(r)\sin(k'r)r^2 \mathrm{d}r$$

with the notation $V(k, k') = \langle k'|V|k\rangle$. The Yukawa potential in momentum basis is therefore

$$V(k, k') = V_\eta \int_0^\infty j_0(kr)\frac{\exp(-\eta x)}{x}j_0(k'r)r^2 \mathrm{d}r$$

$$= \frac{V_\eta}{2\mu kk'} \int_0^\infty \mathrm{d}x\,(\cos\alpha x - \cos\beta x)\frac{\exp(-\eta x)}{x}$$

with $\alpha = \frac{1}{\mu}(k - k')$ and $\beta = \frac{1}{\mu}(k - k')$. Adding and subtracting 1 lets us write the integral as

$$V(k, k') = \frac{V_\eta}{2\mu kk'}\left[\int_0^\infty \mathrm{d}x\,(1 - \cos\beta x)\frac{\exp(-\eta x)}{x} - \int_0^\infty \mathrm{d}x\,(1 - \cos\alpha x)\frac{\exp(-\eta x)}{x}\right]$$

Using a table of integrals we obtain our desired solution

$$V(k, k') = \frac{V_\eta}{\mu kk'}\ln\frac{(\mu\eta)^2 + (k + k')^2}{(\mu\eta)^2 + (k - k')^2}$$

The Reid potential in momentum basis is simply a sum of its terms in momentum basis.

3. Method

3.1. Discretizing Lippman-Schwinger

The equation (??) can be solved numerically by iteration. To this end it is discretized through a series of steps. The principal value poses a problem due to the limited precision of computers. To step around this, the integral is rewritten. The function $\frac{1}{k-k_0}$ is even about k_0, hence having parts of the curve above and below the x-axis, meaning

$$\int_{-\infty}^\infty \frac{\mathrm{d}k}{k - k_0} = 0.$$

Breaking the integral into its positive and negative parts and performing the substitution $k \to -k$ in the negative part then yields

$$\int_0^\infty \frac{\mathrm{d}k}{k^2 - k_0^2} = 0$$

The principal value can now be expressed as

$$\mathcal{P}\int_0^\infty \frac{f(k)}{k^2-k_0^2}\mathrm{d}k = \int_0^\infty \frac{f(k)-f(k_0)}{k^2-k_0}\mathrm{d}k$$

The integral is no longer singular at k_0, instead being proportional to $\frac{\mathrm{d}f}{\mathrm{d}k}$, allowing it to be computed numerically.

In particular, [REF] can be recast to the form

$$K(k,k') = V(k,k') + \frac{2}{\pi}\int_0^\infty \mathrm{d}q \frac{q^2 V(k,q)K(q,k'-k_0^2 V(k,k_0)K(k_0,k')}{(k_0^2-q^2)/m}$$

The integral is approximated through

$$\int_{-1}^1 f(x)\mathrm{d}x \approx \sum_{i=1}^N f(x_i)w_i$$

for N lattice points through the corresponding weights w_i and points $x_i \in [-1,1]$. This is done through Gaussian-Legendre quadrature, using Legendre polynomials to construct the weights and corresponding points. To map the integral from $[-1,1]$ to $[0,\inf]$, the points and weights are transformed by

$$k_i = C \times \tan\frac{\pi}{4}(1+x_i)$$
$$w_i = C \times \frac{\pi}{4}\frac{w_i}{\cos^2\left(\frac{\pi}{4}(1-x_i)\right)}$$

where C is a constant to fix the units.

Applied to our problem, it is discretized into

$$K(k,k') = V(k,k') + \frac{2}{\pi}\sum_{i=1}^N \frac{w_j k_j^2 V(k,k_j)K(k_j,k')}{(k_0^2-k_j^2)/m} - \frac{2}{\pi}k_0^2 V(k,k_0)K(k_0,k')\sum_{n=1}^N \frac{w_n}{(k_0^2-k_n^2)/m}.$$

There are $N \times N$ unknowns for $K(k,k')$, plus 1 for $K(k_0,k_0)$, for a total of $N+1$ unknowns. They can be described by a single extended K-matrix. Defining another matrix A as

$$A_{i,j} = \delta_{i,j} - V(k_i,k_j)u_k$$

with

$$u_j = \frac{2}{\pi}\frac{w_j k_j^2}{(k_0^2-k_j^2)/m} \qquad \text{for } j=1,2,...,N$$

$$u_{N+1} = -\frac{2}{\pi}\sum_{j=1}^N \frac{k_0^2 w_j}{(k_0^2-k_j^2)/m}.$$

Listing 1 The main loop of the K-matrix method.

```julia
function createA(V, k, ω, m)
    N = length(k)-1
    k₀ = k[end]
    A = diagm(0 ⇒ repeat([1.0,], N+1))
    uⱼ = 0.0

    @inbounds for j in 1:N+1
        uⱼ = 0.0
        if j ≠ N+1
            uⱼ = 2/π * ω[j]*k[j]^2/((k₀^2 - k[j]^2)/m)
        else
            for n in 1:N
                uⱼ += ω[n]*k₀^2/((k₀^2 - k[n]^2)/m)
            end
            uⱼ *= -2/π
        end

        for i in 1:N+1
            A[i, j] -= V[i, j] * uⱼ
        end
    end
    return A
end
```

The implementation of this main loop is shown in Section 3.1

The equation can now be rendered as the matrix equation

$$AK = V.$$

Solving for K then simply amounts to inverting A and computing the product

$$K = A^{-1}V. \tag{3.1}$$

As known from [REF], the diagonal of K is proportional to the phase shift

$$K(k_{N+1}, k_{N+1}) = K(k_0, k_0) = -\frac{1}{mk_0}\tan\delta_0(k_0)$$

The number of mesh points N controls both the accuracy and the computation resources, demanding more memory and time as N increases. Running over the $(N+1)\times(N+1)$ matrices scales as roughly $\mathcal{O}(N+1)^2$ in both time and memory allocation. This is the expected behavior to compare to when measuring its actual resource usage.

3.2. Variable Phase Approach

In contrast to the LS approach, implementing the variable phase approach is straightforward. Julia has a very good differential equations solver DifferentialEq.jl[7], which is used for the actual computation. Since the limit in the relation $\delta(k) = \lim_{\rho\to\infty}\delta(k,\rho)$ can not be taken to infinity on a computer, ρ is instead substituted with a very large number, like 5. There is a trade-off between accuracy and computation time, with smaller ρ giving lesser accuracy while taking shorter time to compute, assuming the same step length is being used. To find the optimal ρ, several values were tried and the result compared to a high ρ.

The code implementation is shown in Listing 2

Listing 2 Implementation of VPA in Julia

```julia
struct VPA <: Method
  rspan::Tuple{Float64, Float64}  # Range of the interaction
end
VPA() = VPA((1e-4, 15.0))


function (vpa::VPA)(k, m, V::Potential)
    m = m/2

    function dδdr(δ, p, r)
      -1.0/k * 2.0m * V(r) * sin(k*r + δ)^2
    end

    δ0 = 0.0

    prob = ODEProblem(dδdr, δ0, vpa.rspan)
    sol = solve(prob, maxiters=10000, reltol=1e-8)

    δ = sol.u[end]
end
```

3.3. The Potentials

Two potentials are examined: the square well and the Reid potential. The former has analytical solutions and is relatively simple to understand, and will be used as a check on the implementation of the methods and to illustrate concepts discussed in the theory. The latter is more complicated, being a sum of three Yukawa potentials with the intent on modeling NN-interactions, with coefficients fitted to data.

Their precise implementation is not interesting, but is available in the file potentials.jl.

4. Results and Discussion

4.1. The Square Well Potential

The square well has an analytical form for the phase shift which can be compared to the result of VPA. A well with the arbitrary depth of 4 MeV is used as example, with the computed curves shown in Fig. 2.1. The curves overlap, but the analytical solution has a jump at ≈ 2.8 MeV, stemming from the inherent modulo π ambiguity. The transformation $k \cot \delta$ lifts this ambiguity while fixing the phase shift to 0 at $k = 0$, plotted in the lower panel of the figure. Once transformed the curves overlap perfectly, as expected.

The simple form the square well potential allows us to illustrate some general behaviors of the phase shift. The phase shifts produced by several different well depths are plotted in Fig. 4.2 together with the corresponding cross sections in the lower panel. As $k \to 0$, all curves approach an integral multiple of π, and decrease towards zero as $k \to \infty$. As Levinson's theorem dictates, the multiple of π corresponds to the number of bound states each well can contain, with the number of states increasing as the potential depth increases.

For some particular well depths, the cross sections shot up beyond the limits of the plot. The phase shift curves too have a characteristic shape, rising rapidly near $k = 0$. Examples are marked by dashed lines. Such curves indicate that the potential is on verge of allowing for an additional bound state. [cont]

A related phenomenon happens where the phase shift crosses $\delta = \pi$, at which point the cross section falls off to zero. This is more clearly demonstrated in Fig. 4.3. A phase shift of $n\pi$ means the wave inside the well has precisely n more oscillations than the free wave. When the scattered wave exits the potential, it is exactly in phase with the free wave, and hence indistinguishable. If the higher $l > 0$ waves are negligible in the same region, the potential
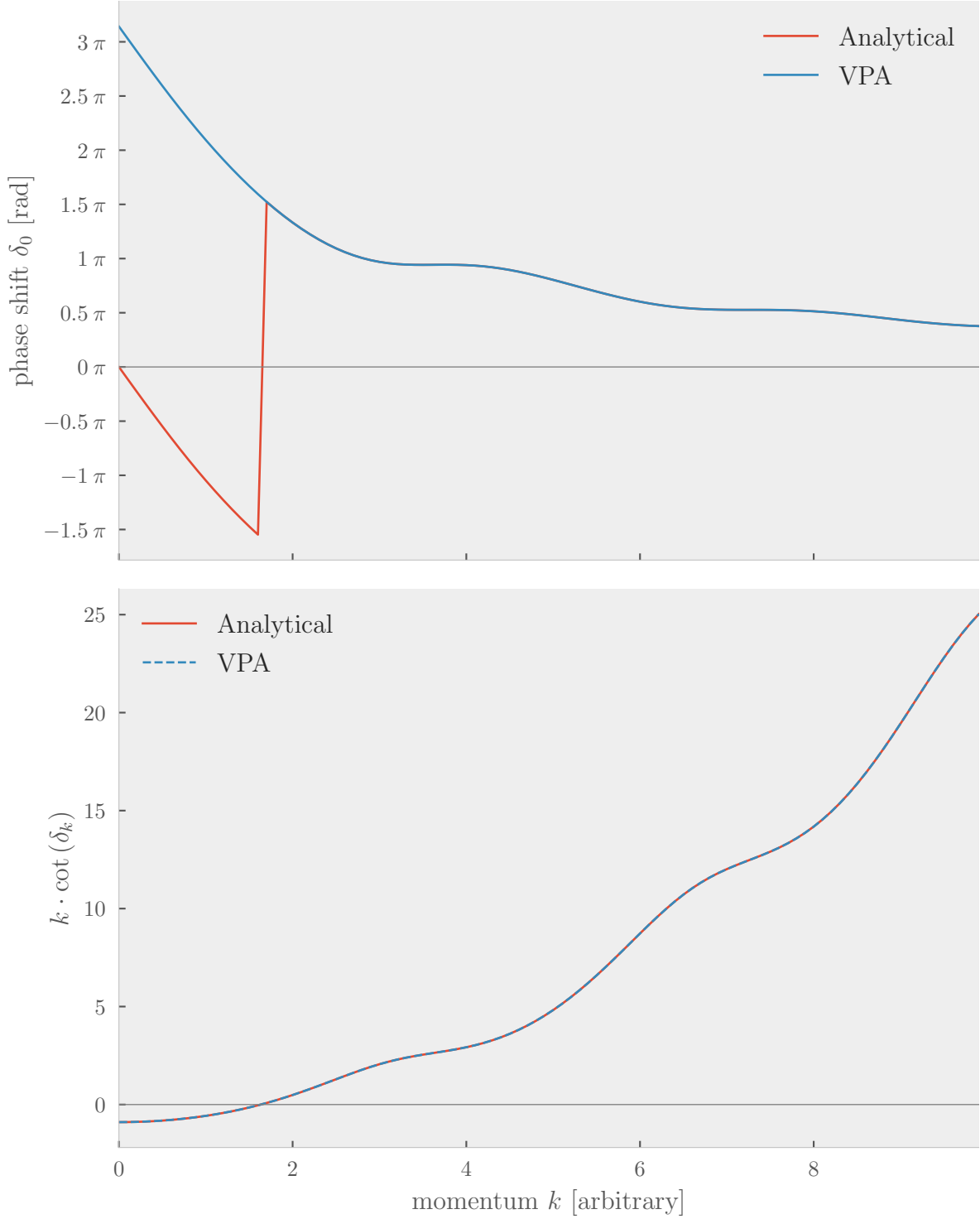
Figure 4.1: The S-wave phase shift for a square well potential $V = -4$ MeV, and reduced mass of 1 MeV. The π-ambiguity in the analytical solution is lifted in the lower panel with the transformation $k \cot \delta_0$, showing a perfect overlap.

causes no scattering at all. This is the cause for the Ramsauer-Townsend effect[1, p. 195], where certain gases are completely transparent for electrons at a given energy.

For completeness sake, the phase shift is found for positive wells, see Fig. 4.4. We expect there to be no bound states, and for the phase shift to be negative. This is indeed the case,
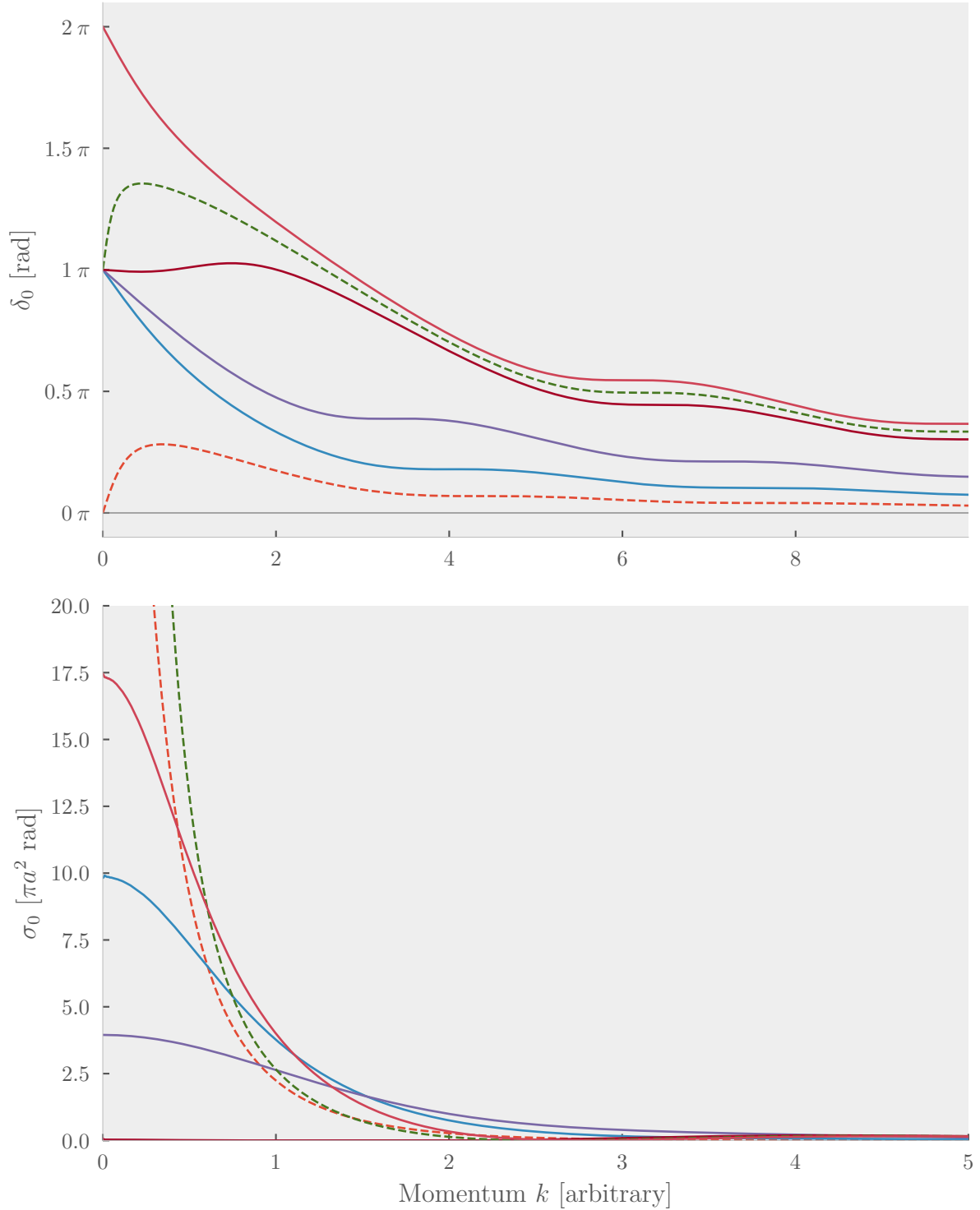
Figure 4.2: The phase shift and corresponding cross section for several square wells of differ-
          ent depths. All curves fall off to zero due to the potential becoming negligible.
          As the wells deepen, the number of possible bound states increases, manifesting
          as curves starting at multiples of π. The dashed lines show the zero energy
          peaks.
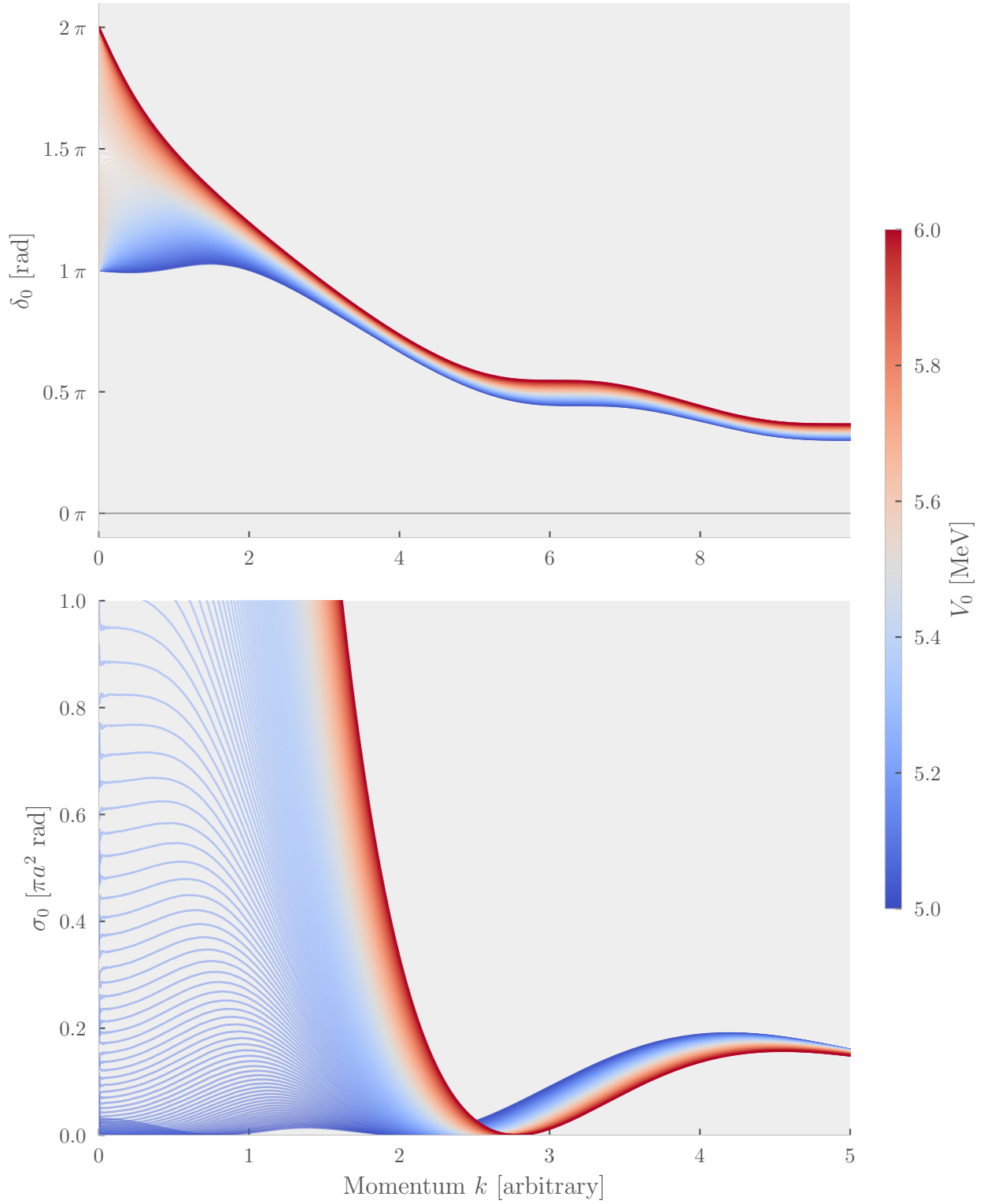
Figure 4.3: Examples of phase shift curves crossing $\delta = \pi$. The scattered wave gets in phase with the free wave, hence equivalent with no scattering. The cross section therefore plummets to zero, as is apparent.

as the figure shows. The step-like behavior is due to the [cont. Skip this section? Kinda obvious. Well, the step behavior is not, but is also not interesting.].
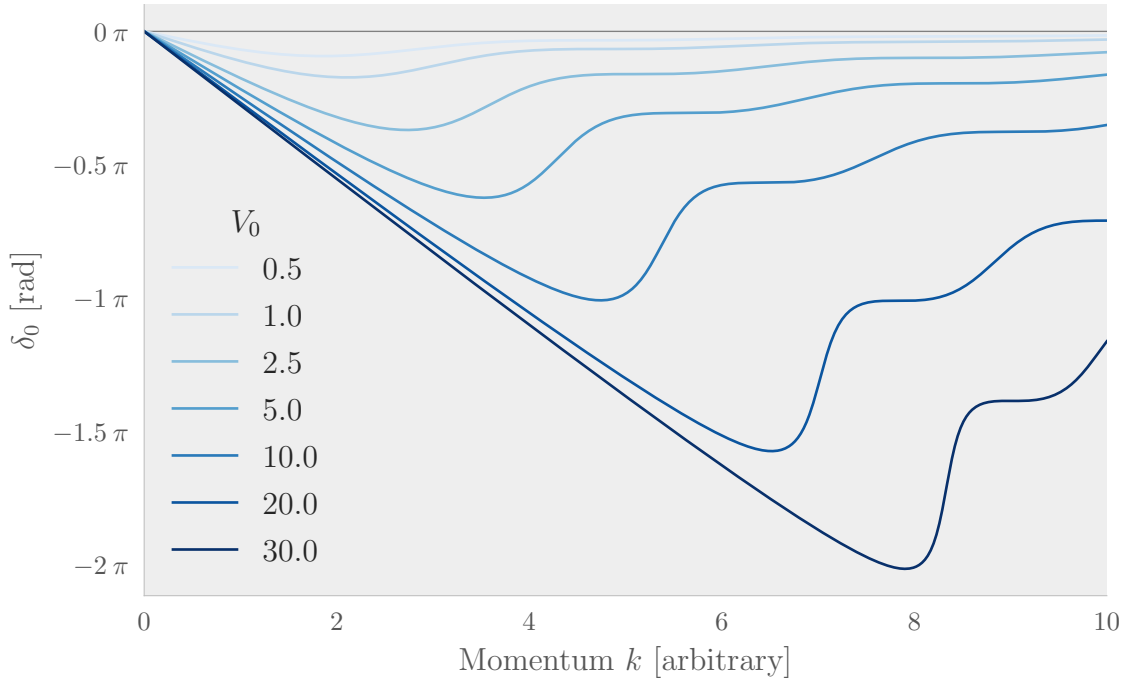
Figure 4.4: The square well with positive well depths, yielding negative phase shifts and no bound states.

4.2. The Reid Potential

4.2.1. K-Matrix

The phase shifts for the $^1S_0$ partial wave of np-scattering obtained through the K-matrix method is shown in Fig. 4.5. This is compared to experimental data from the Nijmegen group[8], also shown in the same figure. There is generally a good agreement, with all features of the experimental data being replicated; a rapid rise from 0 to $\approx 60°$, followed by a fall and a sign flip at ≈ 250 MeV. However, the computed phase shift is consistently lower than the experimental, until they cross.

The accuracy of the K-matrix calculations depends on the number of mesh points used. To determine its influence, the Nijmegen data was interpolated with linear interpolation, and compared to K-matrix calculations using different mesh sizes. The comparison was made by taking the total mean square error (MSE). See Fig. 4.6. As the shape of the curve remains fairly consistent, the MSE of the region $0 \leq T_{\text{lab}} \leq 150$ MeV was chosen as representative of the "total" MSE. This is mainly done to avoid the crossing which slightly complicates the error comparison.

Unsurprisingly, the MSE starts off jumping before quickly falling off to a minimum at about 25 mesh points. As the MSE converges with just a few mesh points, the discrepancy observed in Fig. 4.5 can not be attributed to the method itself. Increasing the number further gives negligible improvements. There is, however, an increasing cost in computational resources.
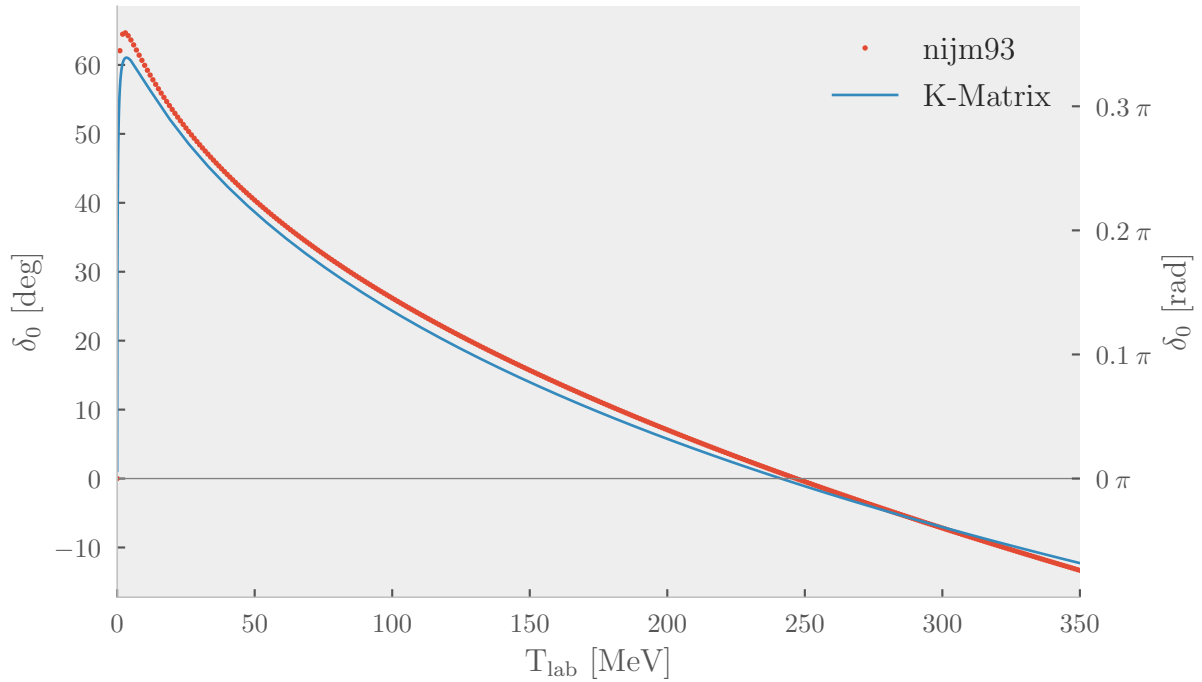
Figure 4.5: Phase shift for $^1S_0$ partial wave of np-scattering, both experimental data from[8] ($nijm93$) and from K-matrix calculations. There is good agreement, but the calculated phase shift is consistently lower than the experimental values. 30 mesh points were used in the calculation for each phase shift point.

The total computation time and amount of allocated bytes used by the K-matrix method is shown in Fig. 4.7. As discussed in Section 3.1, both the time and the memory is expected to increase by roughly $\mathcal{O}(N^2)$. Fitting second degree polynomials, we see that this is indeed roughly the case, with the required time being slightly chaotic. The time was measured by repeating each calculation ten times and taking the median.

There is therefore a trade off between the resources required for a calculation and the accuracy obtained, a trade off which quickly gets increasingly poor, as no further benefit is obtained after ≈ 25 mesh points.

4.2.2. VPA

The second method for obtaining the phase shift from the Reid potential is the variable phase approach. The results are compared with the Nijmegen data in Fig. 4.8, and not unexpectedly, it gives very similar results as Fig. 4.5.

VPA requires the cut-off of the potential to be sufficiently close to infinity to make the error negligible. Cutting off too quickly can be computationally beneficial, so there is one more a trade off between accuracy and resource usage. The resulting phase shifts from different cut-off points are shown in Fig. 4.9. When the cut-off is too small, the potential is effectively a repulsive potential, hence giving a negative phase shift. The phase shift gets increasingly negative as the interaction "sees" more of the repulsive region, but once the attractive region is included, the phase shift quickly increases and converges to the far-away solution ($r_{\text{end}} = 15$).
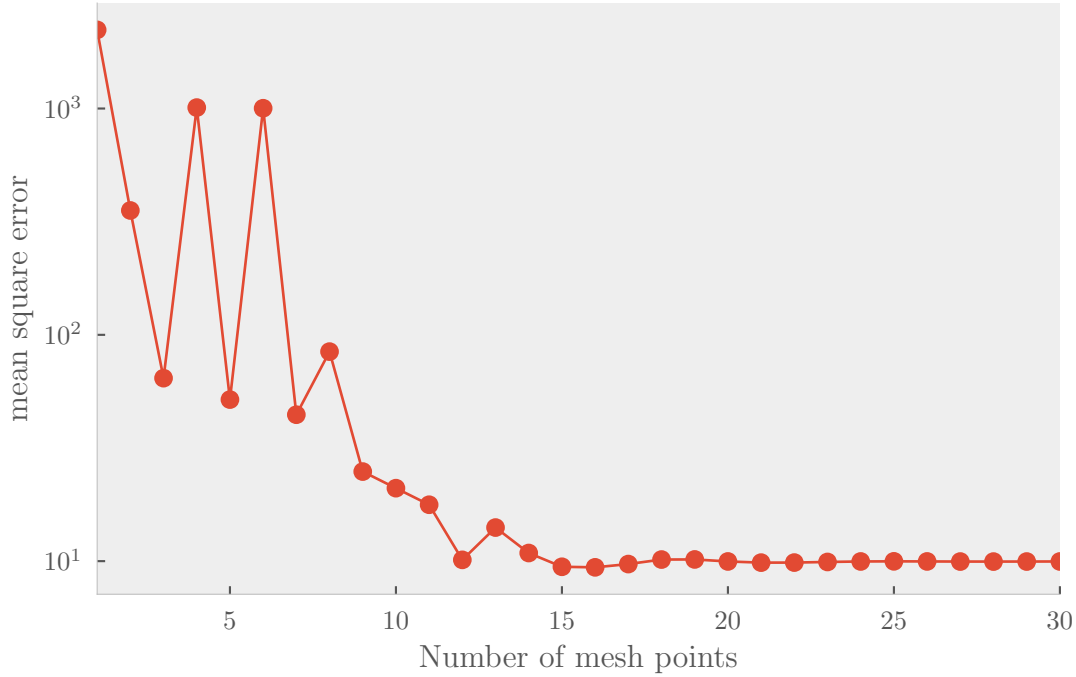
Figure 4.6: The accuracy of the K-Matrix method as a function of number of mesh points. For $n > 20$, the error remains near constant. 150 phase shifts were calculated for energies $0 \leq T_{\text{lab}} \leq 150$.

The resource usage of VPA is significantly more difficult to measure, as the differential equation is solved by the external package DifferentialEq.jl, allowing for a range of different parameters and methods. For completeness sake, the MSE, time and memory usage as a function of the step size is shown in the appendix Fig. A.1. The interesting information is that the time is nearly constant at ≈ 0.2 seconds for the same number of phase shift points as the K-matrix method solved in Fig. 4.7. The K-matrix method is therefore significantly faster, with no loss in accuracy.

4.2.3. Comparison & Exploration

The phase shift from both K-matrix calculations and VPA are plotted together in Fig. 4.10 alongside the experimental data. The pointwise relative error is shown in the lower panel, having a parabolic shape. The theoretical points are perfectly overlapping. Since we already know that VPA is in agreement with the analytical solutions of the square well, we have confidence that the K-matrix method too is correctly implemented.

As the discrepancy between the theoretical computations and the experimental data can be attributed to neither the parameters of the methods nor the methods themselves, the culprit must be the model. The Reid potential was fitted to np-scattering data from the 60s and earlier, while the Nijmegen data is more complete and obtained from more accurate methods.

The phase shift curve of the Reid potential has a striking resemblance to the dashed curves of Fig. 4.2. From our earlier discussion, it is easy to suspect there to be a bound state if the potential was just slightly more attractive. To examine this, the second term of the Reid
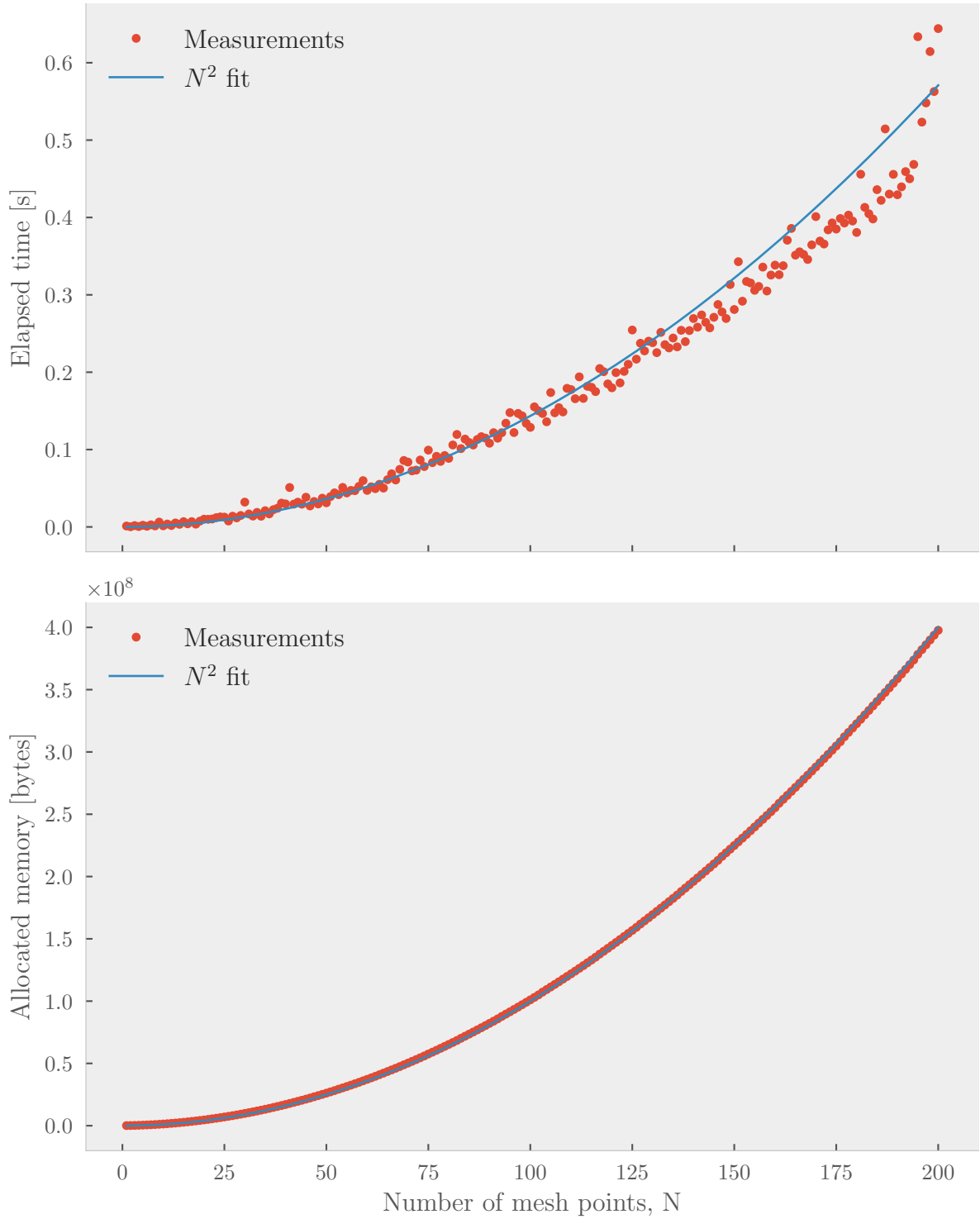
Figure 4.7: Resource usage of the K-matrix method as a function of number of mesh points. The time shows the median of 10 repetitions.

potential was increased by a few percent, yielding the phase shift curves of Fig. 4.11. At +3.37% its strength, the phase shift at $k = 0$ jumps up to 180°, allowing for a bound state by Levinson's theorem.
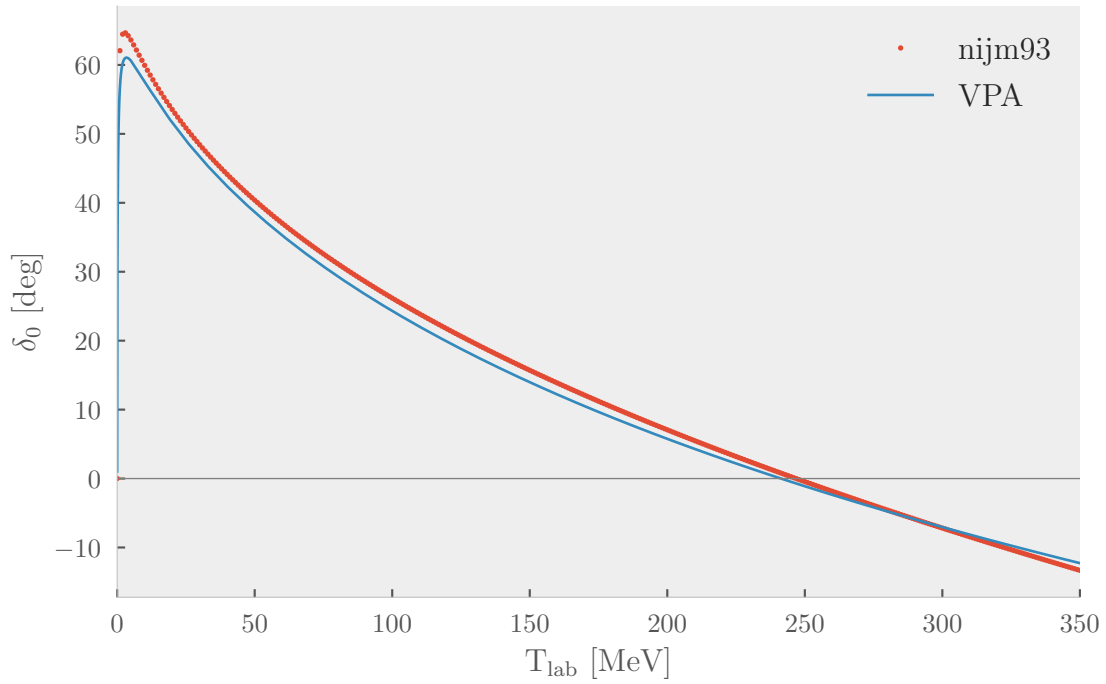
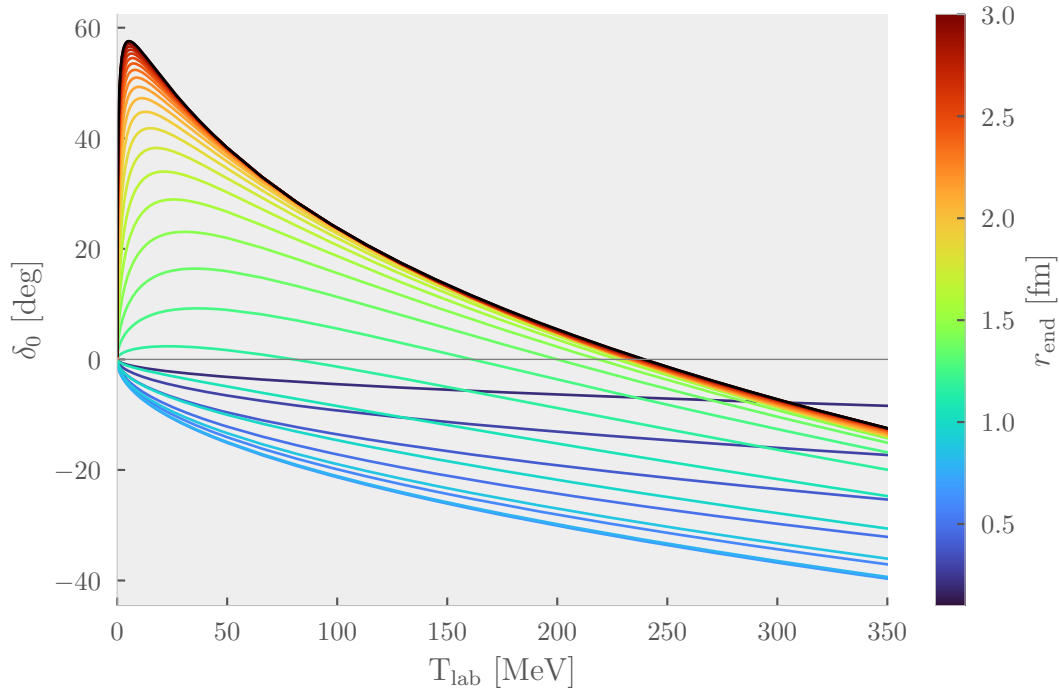Figure 4.8: The resulting *S*-wave phase shift from variable phase approach alongside experimental data.

Figure 4.9: The effect of using different cut off points r_{end} of the potential. Note how the different cut off points correspond to the different radii of Fig. 2.2.
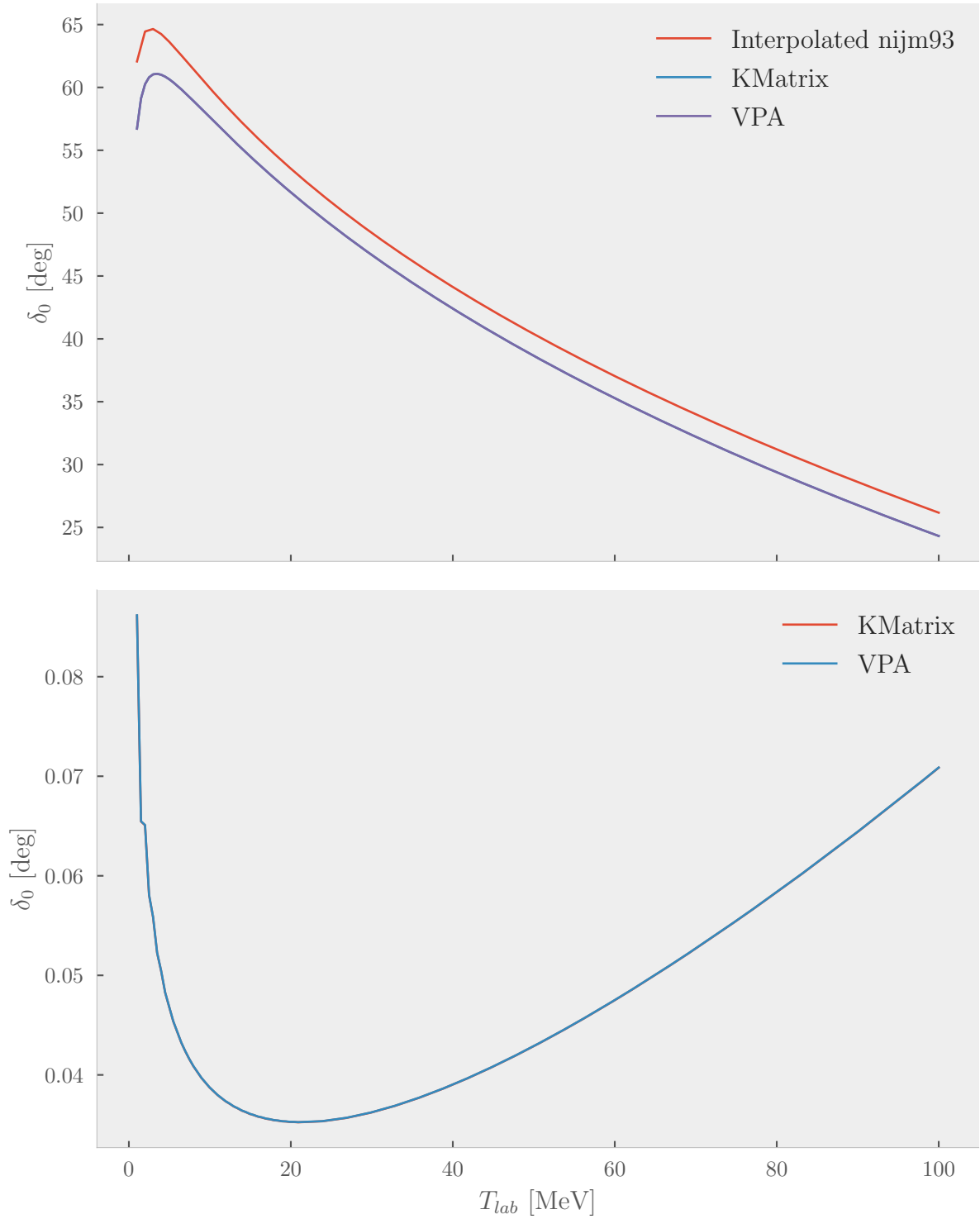
5. Conclusion

Figure 4.10: The results of K-matrix and VPA using good parameters, compared to the $nijm$93 data. The relative error is shown in the lower panel. Only $1 < T_{\text{lab}} < 100$ MeV are included; an arbitrary choice to exclude the jump at ≈ 0.1 MeV and the crossing near 250 MeV.
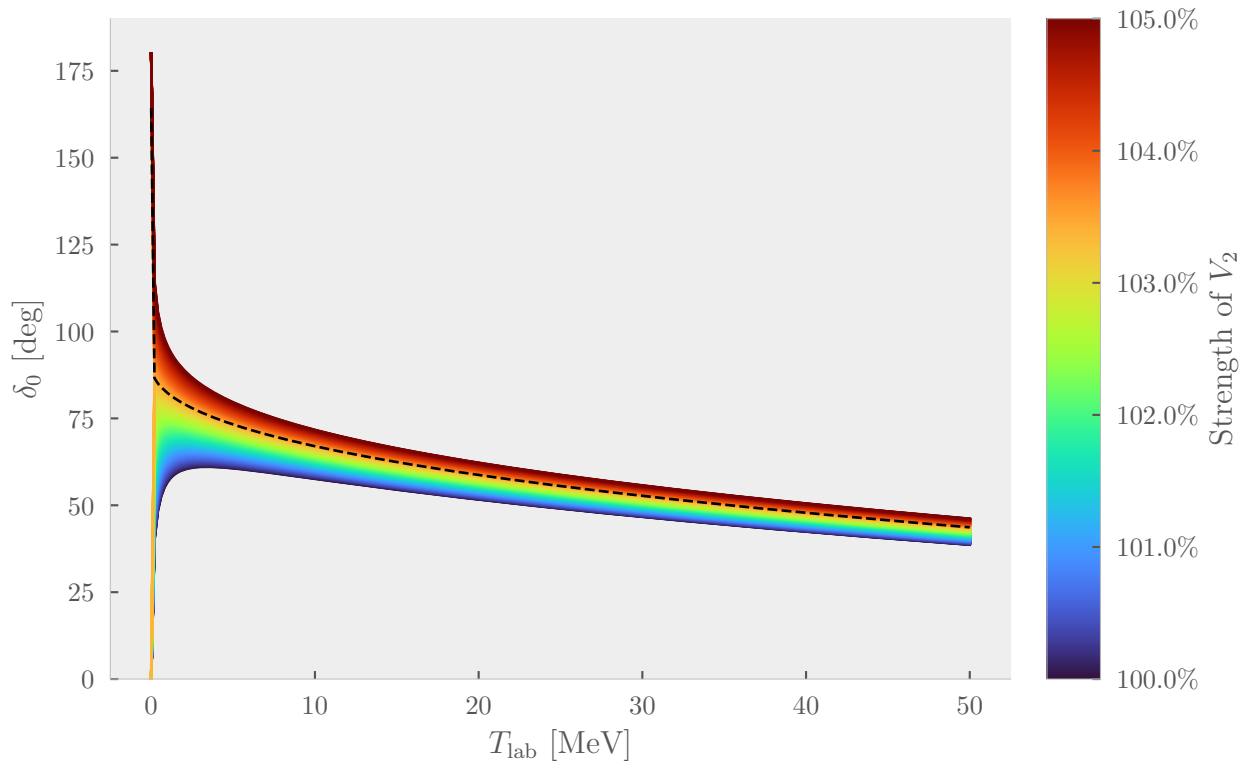
Figure 4.11: The phase shift curves resulting from making the Reid potential more attractive by increasing the strength of its second term ($V_2 = -1650.6$ MeV). The initial blue 100% denotes its original value. At a 3.37% increase, the curves no longer begin at 0°, but jump to 180°. This is marked by a dashed line. The apparent lower start point is due to numerical inaccuracy.

References

[1] R. John Taylor. Scattering Theory. John Wiley & Sons, Inc., 1972 (cit. on pp. 1, 2, 5, 8, 10, 11, 18).

[2] Albert Messiah. Quantum Mechanics. John Wiley & Sons, Inc., 1961 (cit. on p. 6).

[3] Eric C. Le Ru, Walter R. C. Somerville, and Baptiste Auguié. "Radiative correction in approximate treatments of electromagnetic scattering by point and body scatterers". In: Physical Review A 87.1 (Jan. 2013). DOI: 10.1103/physreva.87.012504. URL: https://doi.org/10.1103%2Fphysreva.87.012504 (cit. on p. 7).

[4] Laszlo Szunyogh. "Introduction to Multiple Scattering Theory". Short text obtained through the web. URL: http://newton.phy.bme.hu/~szunyogh/Elszerk/Kkr-slides.pdf (cit. on p. 8).

[5] Unknown. "Chapter 3 - Integral form of the Schrödinger equation". Excerpt from unknown book. Clearly explains the reasoning behind the reactance matrix. URL: http://shodhganga.inflibnet.ac.in/bitstream/10603/68621/9/09_chapter%5C%203.pdf (cit. on p. 8).

[6] Roderick V Reid. "Local phenomenological nucleon-nucleon potentials". In: Annals of Physics 50.3 (1968), pp. 411–448. ISSN: 0003-4916. DOI: https://doi.org/10.1016/0003-4916(68)90126-7. URL: http://www.sciencedirect.com/science/article/pii/0003491668901267 (cit. on p. 12).

[7] Christopher Rackauckas and Qing Nie. "Differentialequations.jl–a performant and feature-rich ecosystem for solving differential equations in julia". In: Journal of Open Research Software 5.1 (2017) (cit. on p. 16).

[8] V. G. J. Stoks et al. "Partial-wave analysis of all nucleon-nucleon scattering data below 350 MeV". In: Phys. Rev. C 48 (2 Aug. 1993), pp. 792–815. DOI: 10.1103/PhysRevC.48.792. URL: https://link.aps.org/doi/10.1103/PhysRevC.48.792 (cit. on pp. 21, 22).
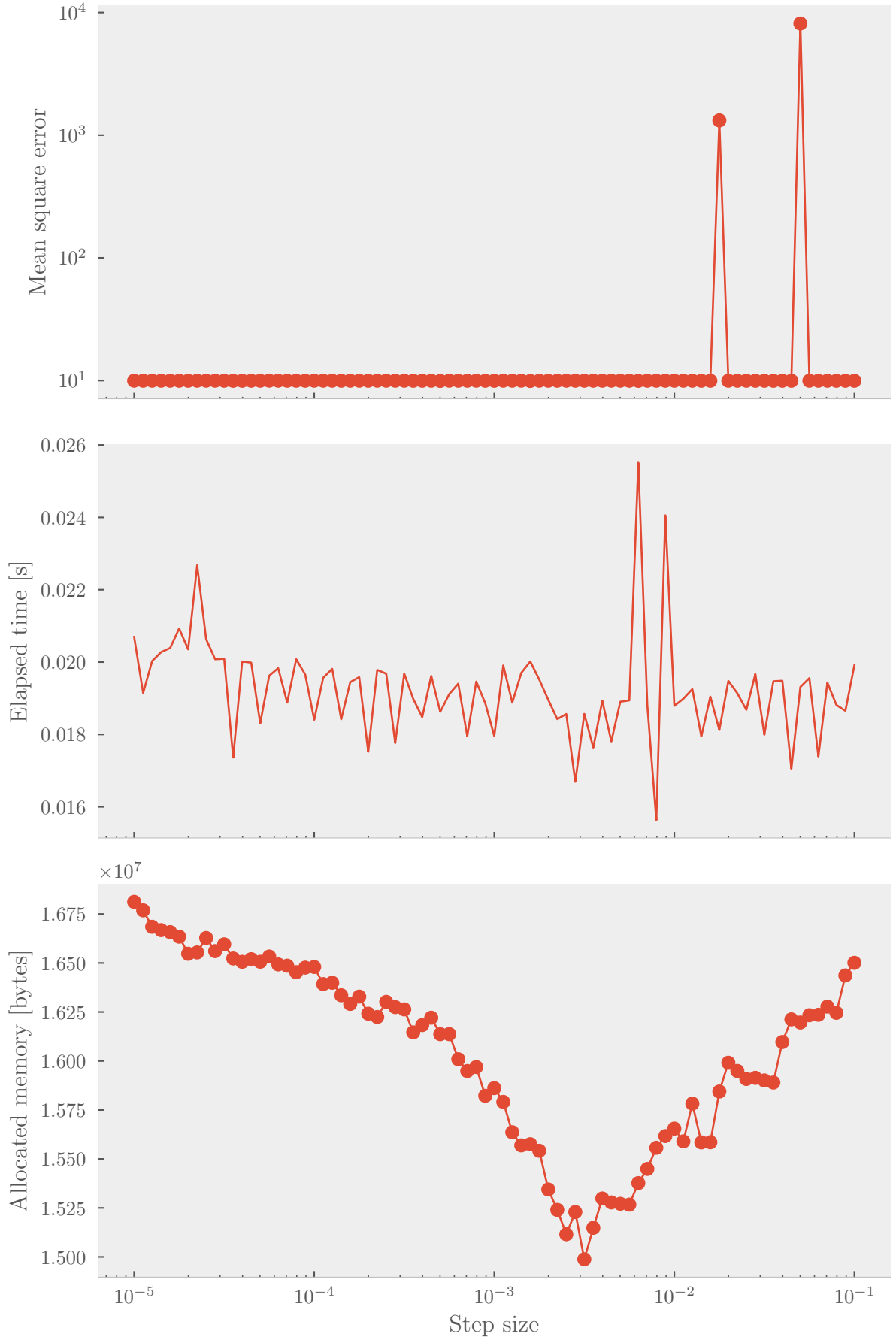
Appendices

Figure A.1: Mean square error and resource usage of VPA as a function of step size of the solver. Only allocated memory has a significant change, reaching a minimum at 0.008
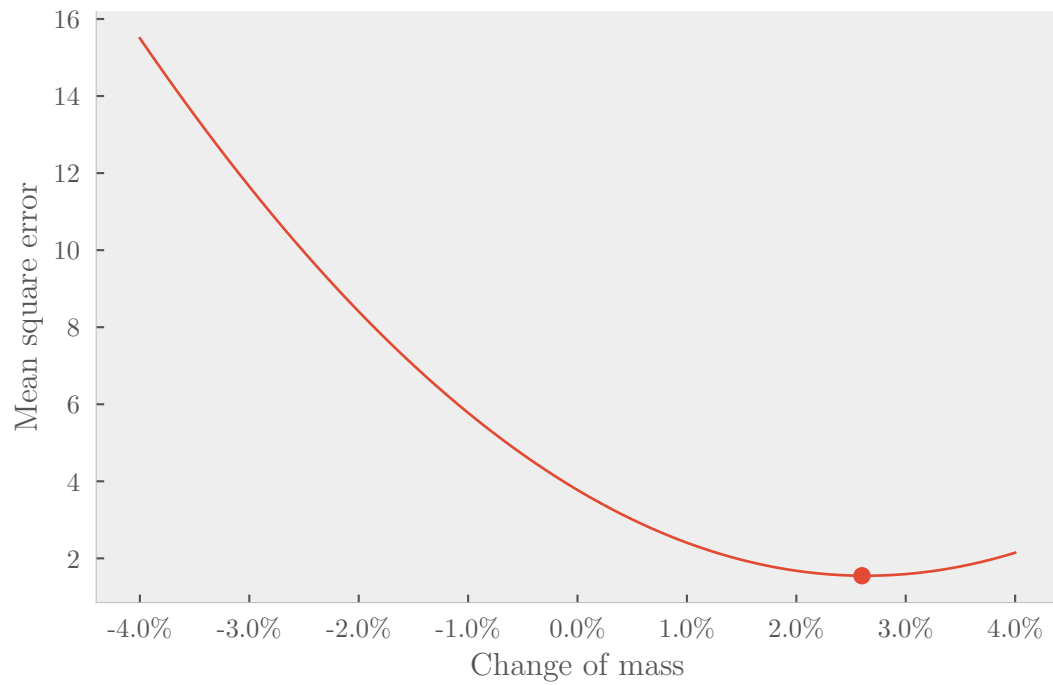
Figure B.1: The total MSE of each model using different mass. The minimum occurs at an additional $+2.6\%$ mass, $481.9\,\mathrm{MeV/c^2}$.